ANTIOXIDANTS & REDOX SIGNALING
Volume 8, Numbers 9 & 10, 2006

Forum Original Research Communication

Single-Cell Optical Imaging of the Phagocyte NADPH Oxidase

HENK-JAN VAN MANEN,[1] ROBIN VAN BRUGGEN,[2] DIRK ROOS,[2] and CEES OTTO[1]

ABSTRACT

The phagocyte NADPH oxidase is a key component of the innate immune response against invading microorganisms, because the generation of superoxide (O_2^-) inside the phagocytic vacuole by this enzyme is responsible for microbial killing by mechanisms that are directly or indirectly dependent on reactive oxygen species (ROS) formation. Most of what is known about the membrane-embedded and cytosolic NADPH oxidase subunits and their intricate network of interactions on assembly and activation has been derived from biochemical and biophysical studies involving subcellular fractionation or reconstituted cell-free systems. Such investigations can be complemented by single-cell microscopy on phagocytes, which may reveal spatial and/or temporal details about NADPH oxidase assembly that cannot be obtained from fractionated-cell assays. In recent years, we have investigated the NADPH oxidase in neutrophils using two complementary optical imaging techniques: Raman microscopy, a vibrational spectroscopic technique that does not require protein labeling, and live-cell fluorescence microscopy, which sheds light on the dynamics of NADPH oxidase assembly in individual cells. Here, we briefly introduce these techniques, compare their characteristics, and show their potential for studying NADPH oxidase at the single-cell level. New microscopy data are presented to illustrate the versatility of Raman and fluorescence microscopy on intact neutrophils. *Antioxid. Redox Signal.* 8, 1509–1522.

INTRODUCTION

PROFESSIONAL PHAGOCYTES such as neutrophils, macrophages, and dendritic cells are crucial in immune and inflammatory responses against infections by virtue of their ability to recognize and engulf invading microorganisms (86, 88). Whereas neutrophils and macrophages have an essential role in innate immunity by killing and degrading the internalized microbes inside phagolysosomes (55, 97), dendritic cells and also macrophages use phagocytosis to induce a long-term adaptive immune response and protection by presenting microbial antigens on their surface to specific T lymphocytes (86). As this article is concerned mainly with the innate immune response of neutrophils, the involvement of professional phagocytes in adaptive immunity is not further discussed here.

Being able to leave the bloodstream and migrate to sites of infection by chemotaxis, neutrophils form an important line of defense against invading microbes. After phagocytosis, they expose pathogens in the phagosome to destructive reactive oxygen species (ROS) and hydrolytic proteins that are liberated from granules. It has been known for more than 25 years that bactericidal ROS are derived from the superoxide-producing enzyme NADPH oxidase (reviewed in refs. 6, 21, 76, 98). The membrane-embedded, catalytic subunit gp91^{phox} of this enzyme transports electrons across the phagosomal or plasma membrane, resulting in the one-electron reduction of oxygen to superoxide (O_2^-). However, recent work indicates that NADPH oxidase also mediates the activation of microbicidal proteases in the phagolysosome (72, 78). The release of electrons into the phagosomal lumen, as a result of NADPH oxidase activity, leads to a compensating influx of cations

[1]Biophysical Engineering Group, Faculty of Science & Technology, Institute for Biomedical Technology (BMTI), and MESA$^+$ Institute for Nanotechnology, University of Twente, Enschede, The Netherlands.
[2]Department of Blood Cell Research, Sanquin Research, and Landsteiner Laboratory, Academic Medical Centre, University of Amsterdam, Amsterdam, The Netherlands.

such as H^+ and K^+, through a voltage-gated proton channel (25), believed by some investigators (41) but not by others (24) to be gp91^{phox}, and a large-conductance Ca^{2+}-activated potassium channel (1), respectively. The increase in potassium ion concentration in the phagocytic vacuole liberates and activates proteases from the acidic proteoglycan matrix of neutrophil granules that have fused with the phagosome. Thus, efficient bacterial killing, by both ROS generation and protease activation (71), is critically dependent on NADPH oxidase activity. This is apparent from studies with neutrophils from patients with chronic granulomatous disease (CGD), in which a dysfunctional NADPH oxidase caused by a genetic defect in one of its subunits leads to recurrent and life-threatening infections (44, 75).

For the past two decades, intensive research efforts have been undertaken to identify the crucial NADPH oxidase subunits in phagocytes and to unravel the mechanisms that are responsible for regulating the onset, intensity, and termination of NADPH oxidase activity under a variety of conditions. We here provide the following summarizing statements about NADPH oxidase structure, assembly/activation, and regulation, and refer the reader to recent in-depth reviews for detailed discussions (6, 21, 26, 70, 76, 98):

1. The catalytic core of NADPH oxidase consists of flavocytochrome b_{558} (further referred to as cyt b_{558}), a heterodimeric membrane protein consisting of gp91^{phox} and p22^{phox} (*phox, ph*agocyte *ox*idase). The 91-kDa gp91^{phox} subunit is a flavohemoprotein that contains binding sites for NADPH, FAD, and heme prosthetic groups (in a 1:1:2 ratio) that take part in the electron-transporting catalytic cycle. The small subunit p22^{phox} is a stabilizing membrane protein for gp91^{phox} and a docking site for cytosolic subunits that are indispensable for *in vivo* NADPH oxidase activation.
2. In resting neutrophils, NADPH oxidase is unassembled and therefore dormant because of the separation between membrane-bound (cyt b_{558}) and cytosolic (p47^{phox}, p67^{phox}, p40^{phox}, and Rac) subunits. Activation of cells by soluble or particulate stimuli leads to translocation of the heterotrimeric p47^{phox}–p67^{phox}–p40^{phox} complex from the cytosol to the cyt b_{558} in the plasma membrane or phagosomal membrane. This translocation depends on extensive phosphorylation of p47^{phox} by protein kinases (most notably isoforms of protein kinase C), leading to a conformational change that relieves p47^{phox} from its autoinhibited state and allows it to dock onto membrane-bound p22^{phox}.
3. Whereas p47^{phox} has an organizing function, mainly by bringing p67^{phox} in close proximity to gp91^{phox}, p67^{phox} is absolutely indispensable for NADPH oxidase activity because it contains an activation domain that is critical for electron transport through and thus superoxide production by gp91^{phox}.
4. Rac (Rac1 in macrophages, Rac2 in neutrophils) is critical for NADPH oxidase assembly and possibly activation. Although Rac1/2 translocates separately from the p47^{phox}/p67^{phox}/p40^{phox} trimer to the plasma and/or phagosomal membrane on cell stimulation, it must bind to p67^{phox} for NADPH oxidase activity to occur. Whether Rac1/2 has only an organizing (like p47^{phox}) or also an activating function in electron transport is currently under debate (10).
5. Besides the essential interactions between the *phox* subunits described, many of which have been characterized structurally (36), it is also known that many membrane-bound, lipid second messengers play an important role in regulating NADPH oxidase activity. Among these lipids are arachidonic acid (AA), diacylglycerol, and phosphatidic acid, which are products of phospholipase A_2, C, and D activity, respectively, and several phosphatidylinositol phosphates (PIPs), which are generated by phosphatidylinositol kinases (PIKs), the best studied one in immune cells being phosphatidylinositol 3-kinase (PI3K) (23). These lipid messengers, many of which are also important in phagocytosis and subsequent phagosome maturation (85), exert their effect either directly on NADPH oxidase subunits [for example, both p47^{phox} and p40^{phox} contain PX domains that bind directly to PIPs (65)] or indirectly by stimulating signaling pathways that occur upstream of NADPH oxidase activation.
6. The architecture of the NADPH oxidase (*i.e.*, the separation between membrane-bound and cytosolic subunits in the dormant state) implies that tight spatiotemporal regulation of its activity is important *in vivo*. Indeed, accidental or excessive production of ROS may lead to, for example, inflammatory tissue injury, carcinogenesis, atherosclerosis, and rheumatoid arthritis (7). Moreover, oxidative stress, to which NADPH oxidase-containing microglia (resident macrophages in the brain) may contribute significantly, is increasingly being implicated in neurodegenerative conditions including Alzheimer and Parkinson disease (4, 48).

Almost everything that is known about the membrane-embedded and cytosolic NADPH oxidase subunits and their multitude of interactions on phagocyte stimulation has been derived from biochemical investigations on subcellularly fractionated and reconstituted cell-free systems. Although these approaches have been very successful in dissecting the molecular interactions between NADPH oxidase subunits and signaling pathways leading to oxidase activation, they cannot capture the dynamic protein–protein and protein–lipid interactions that are characteristic and essential for protein activation and regulation processes in living cells. Moreover, weak and transient interactions between components in whole cells may escape detection in experiments on fractionated systems. Thus, analytic tools are needed that reveal spatial and/or temporal details of NADPH oxidase assembly in cellular systems. Here, we present an overview of the microscopic techniques, applied to phagocytes, that have been providing such details. After a brief discussion of well-established microscopic methods, such as electron microscopy (EM) and fluorescence microscopy, which, in combination with immunolabeling or cytochemistry, supply spatial information about NADPH oxidase subunits and ROS production, we focus our discussion on two complementary optical techniques that we have used for NADPH oxidase research at the single-cell level: Raman microscopy on intact neutrophils and live-cell fluorescence microscopy on neutrophil-like PLB-985 cells. As a vibrational spectroscopic tool, Raman spectroscopy provides specific information on endogenous biomolecules (including cyt b_{558}) without the need for protein labeling. We briefly introduce the application of Raman spectroscopy on cells, compare the advantages and limitations of this tech-

nique with those of fluorescence microscopy, and present new Raman spectroscopy and imaging data (see Figs. 3–5) on live and fixed neutrophils, respectively. For fluorescence microscopy on living cells, we have expressed constructs of p67^{phox} and Rac2 labeled with green fluorescent protein (GFP) in human myeloid PLB-985 cells that can be induced to differentiate into *bona fide* neutrophilic phagocytes. These GFP-containing cells can be investigated with sophisticated fluorescence techniques such as fluorescence recovery after photobleaching (FRAP), fluorescence correlation spectroscopy (FCS), and possibly, when two labels are used, Förster resonance energy transfer (FRET), revealing new information about dynamics of and interactions between NADPH oxidase subunits in phagocytosing neutrophils. We illustrate the unique capabilities of these techniques for live-cell studies of the phagocyte NADPH oxidase by discussing new data (see Figs. 6–7) from our groups.

ELECTRON AND FLUORESCENCE MICROSCOPY ON THE PHAGOCYTE NADPH OXIDASE

Localization of NADPH oxidase subunits

In early morphologic studies, high-resolution transmission electron microscopy (TEM) on ultra-thin cell sections was used to distinguish different granules in neutrophils (8, 13) and to determine the kinetics and sequence of their degranulation into nascent phagocytic vacuoles (77). The availability of antibodies against flavocytochrome b_{558} in the late 1980s made it possible to study the subcellular localization of NADPH oxidase with high spatial resolution by immunogold electron microscopy experiments on resting and phagocytosing neutrophils (35, 49). A major result from these investigations, in combination with analyses of subcellular fractions (11, 20), was the finding that about 80% of the cellular cyt b_{558} content is localized in the membranes of specific granules and secretory vesicles in resting neutrophils, and that part of the cyt b_{558} pool translocates to the plasma or phagosomal membrane as a result of degranulation on cell stimulation.

Immunolabeling in combination with wide-field or confocal fluorescence microscopy has also been used extensively to investigate both NADPH oxidase assembly in phagocytes and colocalization of other cellular components with the oxidase. DeLeo *et al.* (27) monitored association of p47^{phox} and p67^{phox} with cyt b_{558} at the phagosomal membrane by recording immunofluorescence images at fixed time points and demonstrated that termination of oxidase activity correlated with disappearance of the cytosolic subunits from the phagosome. Surprisingly, a similar microscopy study from the same group reported the transient recruitment of p47^{phox} and p67^{phox} to the phagosome in neutrophils from patients with cyt b_{558}–deficient (X-linked) CGD (2). Because earlier studies based on subcellular fractionation and cell-free reconstitution systems had failed to demonstrate translocation of cytosolic subunits in X-CGD neutrophils (see, for example, ref. 43), it is clear that using microscopy on intact cells may reveal subtle processes that may be overlooked when using biochemical assays. Allen *et al.* (2) went on to show that on complete internalization of zymosan particles by X-CGD neutrophils, p47^{phox} and p67^{phox} were quickly shed from the phagosome together with F-actin and the actin-binding protein p57, which also is known to bind p40^{phox} (37), reinforcing earlier data suggesting that association of cytosolic *phox* proteins with the cytoskeleton is required for phagosomal membrane targeting and occurs before binding to cyt b_{558}. Recent examples in which immunofluorescence microscopy has been applied to study NADPH oxidase in phagocytes include the colocalization of gp91^{phox} with cytosolic phospholipase A_2 [a required enzyme for oxidase activity (22)] in the plasma or phagosomal membrane of stimulated neutrophil-like PLB-985 cells (80), the recruitment of cyt b_{558} and cytosolic *phox* proteins to lipid rafts [cholesterol-enriched membrane microdomains that function as signaling platforms (83)] in neutrophils primed with interleukin-8 (38), the impaired translocation of cyt b_{558} to the phagocytic vacuole in neutrophils and macrophages infected with the bacterial pathogens *Anaplasma phagocytophilum* (17, 47) and *Salmonella typhimurium* (33, 96), respectively, and the colocalization of neutrophil flavoprotein autofluorescence and gp91^{phox} within 7 nm by FRET (52), strongly suggesting that a significant fraction of neutrophil autofluorescence at 420- to 490-nm excitation is due to NADPH oxidase. Interestingly, with time-resolved spectroscopy, the latter study reported a periodic transient reduction of 54 ± 2 msec in the NADPH oxidase-related flavoprotein autofluorescence, consistent with earlier reports indicating that oscillatory electron transport across the NADPH oxidase enzyme is promoted by propagating waves of the gp91^{phox} substrate NADPH (51). Of note, autofluorescence imaging on neutrophils, used extensively by Petty and co-workers (51), does not require labeling of NADPH oxidase subunits, a feature that this technique shares with resonance Raman spectroscopy (*vide infra*).

Localization of intracellular ROS production

An indirect way to determine the cellular localization of active NADPH oxidase is to visualize the sites of ROS generation. Cytochemical methods for the detection of O_2^- [*e.g.*, nitroblue tetrazolium (NBT) and 3,3′-diaminobenzidine (DAB)/Mn^{2+}] and H_2O_2 (*e.g.*, Ce^{3+}), in combination with electron microscopy (EM), were critical in establishing that ROS production occurs at the plasmalemma/phagosomal membrane of stimulated neutrophils (reviewed in ref. 73). However, with DAB/Mn^{2+} cytochemistry and EM, Kobayashi *et al.* (53) showed that O_2^- generation occurs at intracellular granules in PMA-stimulated neutrophils and not at the plasma membrane (53). This had already been suggested by chemiluminescence and fluorescence assays (59) and was confirmed more recently by fluorescence microscopy with ROS-dependent fluorogenic dyes (15). When combined with results from biochemical studies (3, 50, 90), these findings suggest that on PMA stimulation, NADPH oxidase is activated within intracellular granules that can subsequently be targeted to and fused with the plasma membrane.

The use of fluorogenic compounds such as hydroethidine, dihydrorhodamine-1,2,3, and 2′-7′-dichlorodihydrofluorescein (DCDHF), which become fluorescent on oxidation by ROS, is widespread in phagocyte biology (101). These dyes

serve as sensitive probes in fluorescence microscopy experiments to provide spatial and temporal information about ROS production by phagocytes, thereby reflecting NADPH oxidase activity. However, their use in microscopy or other fluorescent assays is not without limitations (87). The intracellular locations where the fluorescent products accumulate may not necessarily be the site of their production. For example, ethidium, generated as a result of hydroethidine oxidation, is targeted to the nucleus, whereas rhodamine-1,2,3 accumulates in mitochondria. In addition, many probes lack specificity, serving only as a general ROS probe, and some require peroxidase activity for their oxidation to fluorescent species. Nevertheless, through the development of probes with improved ROS specificities, together with better targeting methods, fluorescence-based ROS detection will likely remain a popular method for establishing intracellular NADPH oxidase activity with spatiotemporal resolution.

RAMAN SPECTROSCOPY AND MICROSCOPY ON SINGLE NEUTROPHILS

In recent years, the use of vibrational spectroscopic techniques such as infrared (IR) and Raman spectroscopy has increased remarkably in fields such as biochemistry, structural and cell biology, and tissue diagnostics (16, 19, 28, 40, 56, 66). Technical developments (*e.g.*, in laser-excitation sources, optics, detectors, and data-analysis methods), the commercial availability of vibrational spectroscopic instrumentation, and the realization that the chemical composition and molecular structure of investigated samples can be probed in a label-free manner have all contributed to the current status of vibrational spectroscopy as a unique analytic tool in the life sciences. Before discussing our application of Raman spectroscopy and microscopy to NADPH oxidase in neutrophils, we briefly introduce the Raman technique and compare its characteristics with those of fluorescence microscopy.

In its most general sense, the Raman effect is caused by inelastic scattering of electromagnetic radiation (usually visible light is used) by matter. In an inelastic scattering process, the two colliding particles exchange energy. On collision of a molecule with an excitation photon (with energy $h\omega_{exc}$, Fig. 1), this energy is quantized by the vibrational states ν (Fig. 1) of the molecule.

The energy difference between the incident and the scattered light gives detailed information about the bond types present in the molecule. Raman spectra of molecules show narrow bands that can usually be assigned to specific molecular vibrations. This is a major advantage over fluorescence spectroscopy, in which the typical broad emission bands reveal little about the identity of the molecules under study. Another difference between fluorescence and Raman spectroscopy is that fluorescence emission occurs from an electronically excited state (Fig. 1a), whereas in nonresonant Raman spectroscopy (Fig. 1b), this state (*E*, Fig. 1) is not involved. In practice, this means that particular fluorescent dyes can be used only when suitable wavelengths for their excitation are available, whereas nonresonant Raman spectra of molecules of interest can be obtained at many different wavelengths. In contrast, resonant Raman (RR) spectroscopy (Fig. 1c), like fluorescence, is performed at an excitation wavelength close to the absorption maximum of the molecule under study. This results in a selective increase, up to four orders of magnitude, in the Raman scattering intensity of the absorbing species (the chromophore) (16, 84). The large difference between nonresonant and resonant Raman spectroscopy is illustrated by the average Raman spectra from the cytoplasm of living neutrophils, taken under nonresonant (647 nm, Fig. 2a) and resonant (413 nm, Fig. 2b) conditions.

At 647-nm excitation, Raman bands from, *e.g.*, aromatic amino acids, amide groups, CH_2 moieties (in lipids and proteins), and heme groups in myeloperoxidase (MPO), an abundant enzyme in neutrophils can be observed (Fig. 2a). In contrast, at 413-nm excitation, the Raman spectrum is almost exclusively due to scattering from cyt b_{558}, with a minor contribution from MPO (Fig. 2b). This is because the heme groups in these enzymes display a strong Soret absorption at (cyt b_{558}) or near (MPO) 413 nm, leading to a selective enhancement of their Raman scattering intensity compared with other cellular components that do not absorb at this wavelength.

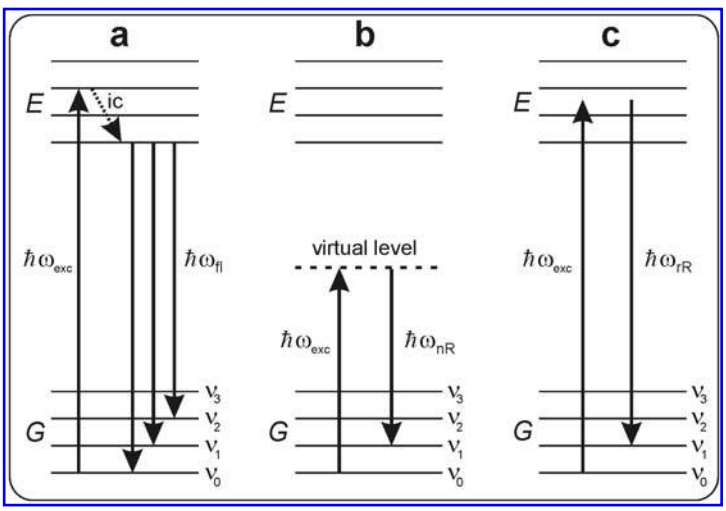

FIG. 1. Schematic energy level diagrams corresponding to fluorescence emission (a), nonresonant Raman scattering (b), and resonant Raman scattering (c). The term *virtual level* is used to describe scattering as an excitation to a state that is lower in energy than a real electronic transition, with a nearly coincident de-excitation and a concomitant change in vibrational energy. Exc, excitation; fl, fluorescence; nR, nonresonant Raman; rR, resonant Raman; G, ground electronic state; E, excited electronic state; ν_i, vibrational states; ic, internal conversion.

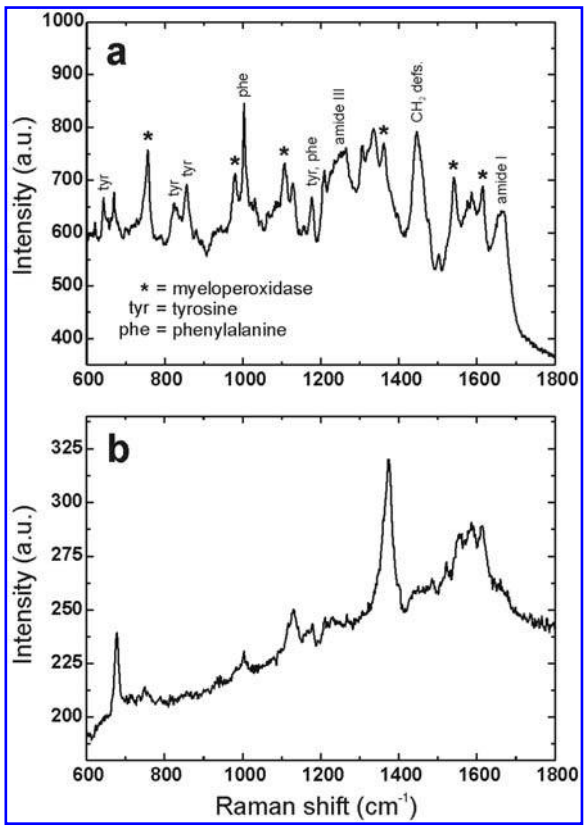

FIG. 2. Nonresonant (a) and resonant (b) Raman spectra of the cytoplasm of living neutrophils. Average spectra from measurements on 10 different cells are plotted. Vibrational bands in the resonant Raman spectrum **(b)** are exclusively from cyt b_{558} and MPO (81). Measurement conditions: **(a)** 15-mW, 647-nm excitation, 30-sec signal accumulation per spectrum; **(b)** 1-mW, 413-nm excitation, 5-sec signal accumulation per spectrum.

Cell and tissue optical-imaging techniques based on Raman spectroscopy have become versatile alternatives to fluorescence microscopy, because vibrational spectra obtained from small intracellular volumes or tissues display a wealth of molecular, specific information, as demonstrated by the Raman spectra from the cytoplasm of neutrophils shown in Fig. 2. In fluorescence microscopy, one must rely on labeling the molecules of interest with fluorophores to obtain the same kind of chemical information. Tedious labeling procedures, and artifacts arising from them, can be avoided in vibrational spectroscopy. Table 1 compares characteristic properties of laser-excited fluorescence and Raman spectroscopy and microscopy.

The high laser powers, long imaging times, and high detection limits reported in Table 1 for Raman spectroscopy are caused by the very low Raman scattering cross-sections of biomolecules compared with the high-absorption cross-sections of molecules used as fluorescent labels in biology. This restricts the use of nonresonant and resonant Raman microscopy to either static situations (*i.e.*, fixed cells) or relatively slow intracellular processes.

Resonant Raman spectroscopy and imaging: label-free visualization of cyt b_{558}

In general, cytochromes and other hemoproteins such as hemoglobin, MPO, and eosinophil peroxidase (EPO) display several strong absorption bands in the visible region of the electromagnetic spectrum. Consequently, many of the structural features of the heme prosthetic groups in these proteins have been unveiled by resonant Raman spectroscopy (84), which reports on, for example, the heme iron redox state, spin state, and axial ligands. Early RR measurements at low temperatures (90 K) on flavocytochrome b_{558} in highly concentrated neutrophil suspensions and solubilized neutrophil plasma membranes were consistent with low-spin, six-coordinate hemes in both ferric (Fe^{3+}) and ferrous (Fe^{2+}) oxidation states (46). By comparison with synthetic models of known constitution, bis-histidine axial ligation of the heme iron centers was suggested. This was confirmed by later RR and electron paramagnetic resonance (EPR) measurements on purified cyt b_{558} at cryogenic temperatures (25 K) (32) and, more recently, by introducing point substitutions in histidine residues that lie within transmembrane domains of $gp91^{phox}$ (9). It is now known that the four histidines involved in axial ligation to the two hemes in $gp91^{phox}$ are strictly conserved among all NADPH oxidase (Nox) family members (54).

In our group, we developed confocal Raman microspectroscopy instrumentation that was, for the first time, sensitive enough to obtain high-quality Raman spectra from individual

TABLE 1. CHARACTERISTIC PROPERTIES OF FLUORESCENCE VERSUS RAMAN SPECTROSCOPY AND MICROSCOPY

	Fluorescence	*Raman*
Excited state lifetime	Long (ns)	Short (ps/fs)
Emission bandwidth	Broad (~40 nm)	Narrow (~0.5 nm)
Typical laser power used for cell imaging*	1–50 μW	0.1–100 mW
Typical cell imaging time*	1–10 sec	15–30 min
Typical image pixel numbers	512 × 512	32 × 32, 64 × 64
Detection limit (molecules)*	1	~10^5 (NR) ~10^3 (RR)
Chemical imaging	After labeling	No labeling required

*Using microscopes available in our laboratories.
NR, nonresonant Raman; RR, resonant Raman.

living cells in a reasonably short recording time (68). Initial experiments at 660-nm excitation revealed that Raman spectra from the cytoplasm of eosinophils and neutrophils were dominated by contributions from proteins and EPO in eosinophils and proteins and MPO in neutrophils (69). Subsequent resonant Raman spectroscopy in the cytoplasm of living normal, MPO-deficient, and cyt b_{558}–deficient (X91^0 CGD) neutrophils showed that, at 413-nm excitation, the Raman signal of neutrophilic granulocytes originates predominantly from cyt b_{558}, with a minor contribution from MPO (81). Because the strong Soret absorption bands of oxidized cyt b_{558} and oxidized MPO are located at 413 nm and 428 nm, respectively, the Raman scattering intensity of these enzymes is enhanced by resonance at 413-nm excitation. Similar measurements after the addition of sodium dithionite, which completely reduces heme groups in cyt b_{558} and MPO to their ferrous (Fe^{2+}) state, led to clear spectral changes in the resonance Raman spectra (81). From these results, we speculated that activation of NADPH oxidase, which is known to involve (transient) reduction of the gp91^{phox} heme groups (discussed in ref. 21), could be followed inside living neutrophils by RR spectroscopy without requiring external labels for ROS detection (*vide supra*). We subsequently demonstrated that stimulation of neutrophils with PMA and *Escherichia coli* bacteria led to changes in the RR spectra that could be assigned to a partial reduction of both cyt b_{558} and MPO (64, 82). Control measurements with cyt b_{558}–deficient (X91^0 CGD) neutrophils failed to show a reduction of intracellular MPO, strongly suggesting that the observed changes in the RR spectra from normal cells on stimulation are due to NADPH oxidase activation. Conclusive evidence, presented here, that this is the case has been obtained using p67^{phox}-deficient (A67^0 CGD) neutrophils. A67^0 CGD cells display normal expression levels of cyt b_{558} and MPO, and RR spectra from unstimulated as well as dithionite-reduced A67^0 CGD cells are identical to spectra from quiescent and dithionite-reduced WT neutrophils (not shown).

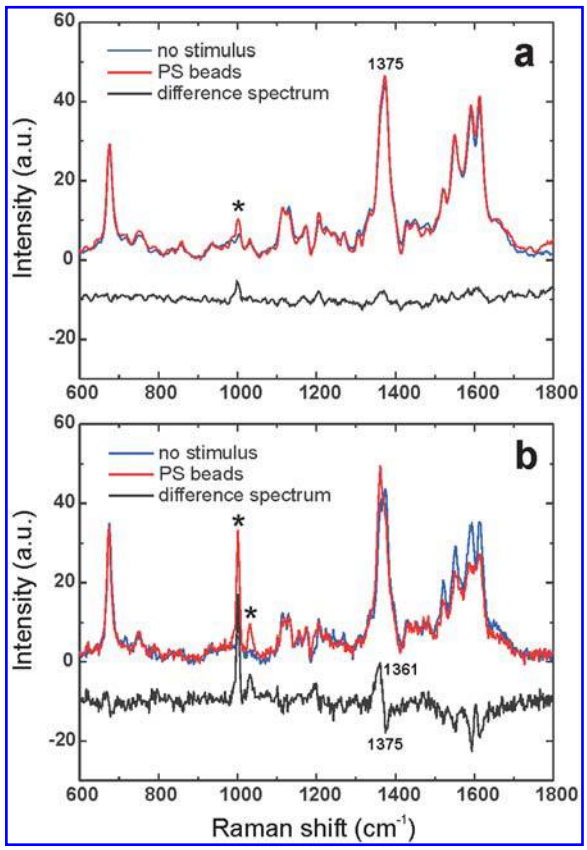

FIG. 3. Resonant Raman spectra from live p67^{phox}-deficient CGD (a) and normal (b) neutrophils showing the absence of cyt b_{558} reduction in p67^{phox}-deficient CGD cells on phagocytosis of serum-opsonized polystyrene (PS) beads. In normal neutrophils **(b)**, the oxidation-state marker band at 1,375 cm^{-1} shifts to 1,361 cm^{-1} on stimulation (see the difference spectrum plotted in black), which is due to a reduction of heme Fe^{3+} to Fe^{2+}. In p67^{phox}-deficient CGD neutrophils **(a)**, the partial reduction of cyt b_{558} is absent in phagocytosing cells. Because NADPH oxidase cannot be activated in these cells, the observed changes in the RR spectra from normal cells **(b)** on stimulation must be due to NADPH oxidase activation. Bands marked with an asterisk in **(a)** and **(b)** are from phagocytosed polystyrene beads. (For interpretation of the references to color in this figure legend, the reader is referred to the web version of this article at www.liebertonline.com/ars.)

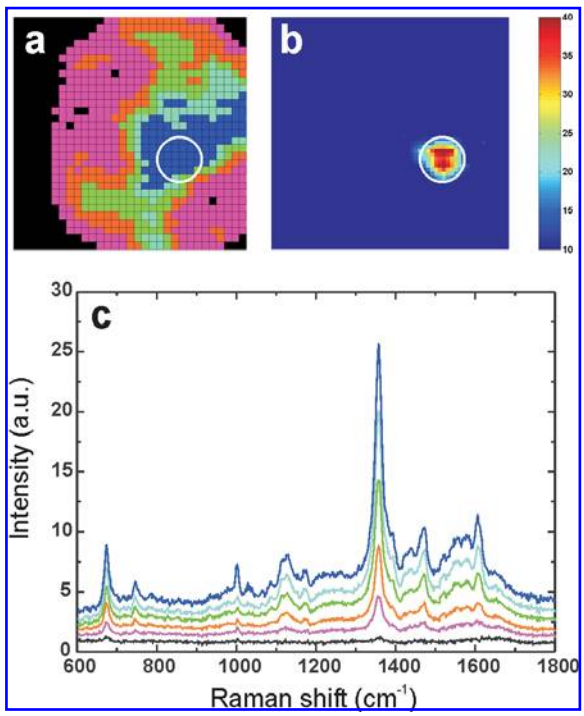

FIG. 4. Resonant Raman microscopy shows the accumulation of cyt b_{558} in the vicinity of a phagocytosed latex bead in a p67^{phox}-deficient CGD neutrophil. (a) RR cluster image (10.4 × 10.4 μm^2) showing the intracellular distribution of cyt b_{558} partitioned into six clusters. **(b)** Corresponding RR image in the 1,001 cm^{-1} vibrational band of polystyrene. **(c)** Average RR spectra extracted from the cluster image displayed in **(a)**. The dark-blue cluster, which surrounds the internalized particle, is highest in cyt b_{558} intensity and accounts for 35% of the total cyt b_{558} pool in the cell. (For interpretation of the references to color in this figure legend, the reader is referred to the web version of this article at www.liebertonline.com/ars.)

However, A67^0 CGD cells that have phagocytosed serum-opsonized latex beads do not show any changes in their RR spectra (Fig. 3a), recorded from a region around the phagosome, whereas in corresponding RR spectra from phagocytosing WT cells, these characteristic changes, indicating a partial reduction of cyt b_{558} and MPO, are clearly observed (Fig. 3b). Moreover, RR spectra of A67^0 CGD cells treated with 50 n*M* PMA, a very potent NADPH oxidase agonist, were identical to RR spectra of unstimulated A67^0 CGD cells (not shown), which is in strong contrast to our previously reported results on WT neutrophils (82).

These findings, proving that electron transfer to the heme groups in cyt b_{558} on NADPH oxidase activation is impaired in p67^{phox}-deficient CGD neutrophils, are consistent with previous biochemical, cell-free experiments, suggesting that the activation domain in p67^{phox} regulates electron transfer from NADPH to FAD (62). A possible way to test this latter suggestion, using living WT and A67^0 CGD neutrophils, might be to perform time-resolved autofluorescence spectroscopy. Kindzelskii and Petty (52) recently used this technique on WT neutrophils to measure the transient reduction in flavoprotein autofluorescence due to electron transport across NADPH oxidase. They found that flavoprotein autofluorescence in activated neutrophils was not reduced on treatment of cells with diphenylene iodonium (DPI), a well-known flavin antagonist, which demonstrates the capability of autofluorescence spectroscopy to monitor electron transport to FAD in NADPH oxidase.

We recently extended our confocal RR spectroscopy studies on neutrophils to the imaging domain by step-wise scanning over single cells while recording full RR spectra at every image pixel (93, 94). From the acquired spectral data sets, confocal Raman images can be constructed by plotting the intensity of a cyt b_{558} Raman band as a function of position. With this method, we visualized the intracellular distribution of cyt b_{558} in both resting and phagocytosing WT neutrophils (93). As expected, part of the cyt b_{558} pool was found to be translocated to latex bead–containing phagosomes, consistent with the well-known degranulation behavior of cyt b_{558}–containing secondary granules and secretory vesicles on phagocytosis (49, 77). We subsequently performed RR imaging experiments on neutrophils treated with PMA (94) and found that most of the cyt b_{558} was located near the cell periphery, which is in line with extensive specific-granule exocytosis that is known to occur on PMA stimulation (30). Examination of the reduced/oxidized cyt b_{558} ratio across PMA-stimulated cells revealed a rather homogeneous distribution of partly reduced cyt b_{558}, reflecting the unpolarized intracellular activation of NADPH oxidase on PMA treatment that has been demonstrated before with cytochemical methods and fluorogenic ROS-sensitive dyes in combination with electron and fluorescence microscopy (see the *Localization of intracellular ROS production* section). In contrast to these latter procedures, RR microscopy is a label-free vibrational spectroscopic technique that can be applied to unpermeabilized cells.

As a final example, we report here that cyt b_{558} also translocates to the phagosome in p67^{phox}-deficient (A67^0 CGD) neutrophils stimulated with serum-opsonized latex beads. The RR cluster image of a phagocytosing A67^0 CGD cell, displayed in Fig. 4a, shows a dark blue cluster of highest average cyt b_{558} intensity (Fig. 4c), which localizes around the phagocytosed latex bead, the RR image of which is displayed in Fig. 4b. The light blue, green, orange, and magenta clusters are of lower intensities (Fig. 4b), demonstrating the accumulation of cyt b_{558} close to the internalized particle.

With cyt b_{558} translocation to the phagosome being normal in these cells, it is likely that the absence of superoxide production in these cells, and thus the impaired bacterial killing, is solely due to a defective electron-transport mechanism through gp91^{phox}, as shown earlier with RR spectroscopy.

We conclude this section by the two following summarizing statements:

1. Confocal resonant Raman spectroscopy offers quantitative and structural information about cyt b_{558} (and MPO) inside unlabeled, living WT and CGD neutrophils. Its application to other cyt b_{558}–containing phagocytes such as macrophages and differentiated PLB-985 cells, as well as to nonphagocyte Nox family members, will further help to elucidate NADPH oxidase activation mechanisms in a variety of cell types.
2. The extension of RR spectroscopy to microscopy allows us to visualize the intracellular distribution of cyt b_{558}, and concomitantly its redox state, in both resting and stimulated WT and autosomal recessive CGD neutrophils. Used in combination with powerful data-analysis methods that have been developed for large spectroscopic data sets (including singular-value decomposition, principal-component analysis, and hierarchical cluster analysis), we believe that RR microscopy is at present a very useful technique in phagocyte biology and CGD research. It also has the potential to become a versatile tool in the characterization of nonphagocyte Nox enzymes.

Nonresonant Raman imaging: visualization of lipid bodies in phagocytosing neutrophils

By comparing the average nonresonant (Fig. 2a) and resonant (Fig. 2b) Raman spectrum from the cytoplasm of living neutrophils, it is seen that nonresonant Raman spectroscopy at 647-nm excitation lacks the specificity for cyt b_{558} that resonant Raman spectroscopy provides. In general, Raman spectra recorded from cells under nonresonant conditions display a multitude of vibrational bands from constituents of endogenous biopolymer classes that are present at high concentrations, such as proteins, nucleic acids, carbohydrates, and lipids. Consequently, vibrational spectroscopy has been applied successfully in cases in which large overall biochemical changes occur in cells and tissues [for example, in apoptosis (89), stem cell differentiation (63), and atherosclerosis (92)]. The recent application of Raman spectroscopy and infrared microscopy to breast cancer diagnosis (39) and histopathologic characterization of prostatic tissue (31), respectively, highlights the increasing importance of vibrational spectroscopy in clinical diagnosis (19).

In nonresonant Raman microscopy studies aimed at visualizing the redistribution of cellular constituents on phagocytosis, we discovered that phagocytic vacuoles were frequently in close proximity to lipid-rich organelles of ~1 μm diameter (95). It is known that an increased number of lipid bodies

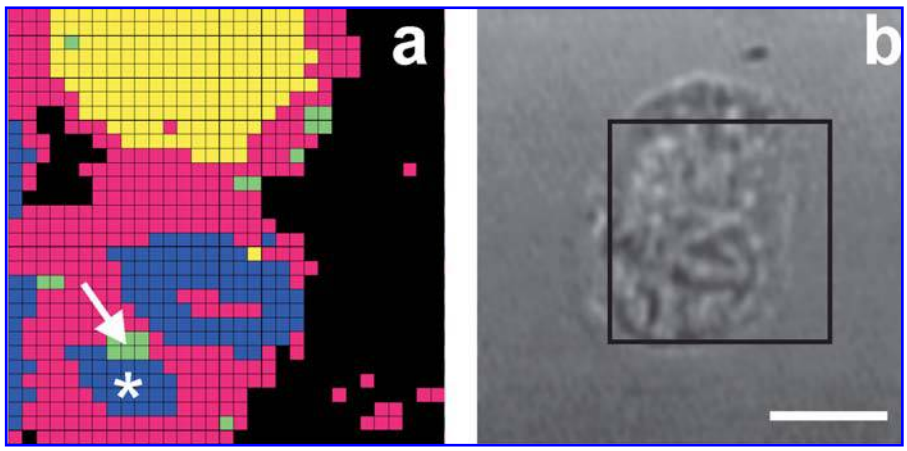

FIG. 5. Nonresonant Raman microscopy shows the association of an arachidonate-rich lipid body (*arrow*) with an internalized zymosan particle in a neutrophil. (a) Raman cluster image (9.4 × 9.4 μm²) showing clusters corresponding to lipid bodies (green), zymosan particles (blue, marked with asterisks), the cytoplasm (magenta), and the nucleus (yellow), as identified by average Raman cluster spectra (not shown). **(b)** Corresponding white-light transmission image. The area enclosed by the black square was used for Raman imaging. The scale bar represents 5 μm. (For interpretation of the references to color in this figure legend, the reader is referred to the web version of this article at www.liebertonline.com/ars.)

(LBs), cytoplasmic inclusions composed mainly of triglycerides, phospholipids, and sterol esters, is usually found in leukocytes engaged in inflammation (reviewed in ref. 12). The presence of LBs in close apposition to phagolysosomes was already noted in electron microscopy studies of macrophages stimulated with zymosan particles (29) or infected with the intracellular protozoan *Trypanosoma cruzi* (60). To study in more detail the association between LBs and phagosomes in neutrophils, we induced the formation of LBs by exposing cells to arachidonic acid (AA). Subsequent Raman microscopy revealed the presence of many LBs rich in unsaturated lipids. Conclusive evidence for the accumulation of exogenously added AA in esterified form in LBs was obtained using octadeuterated AA (AA-d_8). After formation of LBs in neutrophils by AA or AA-d_8 and subsequent phagocytosis of serum-opsonized latex beads, Raman microscopy again showed the accumulation of LBs near internalized particles (95), and we report here that LBs are also present in close proximity to ingested zymosan particles, as exemplified by the nonresonant Raman cluster image shown in Fig. 5.

Interestingly, we further found that the accumulation of LBs near phagosomes is mediated, at least in part, by the NADPH oxidase subunit gp91^{phox}, as markedly different distributions of LB-phagosome distances were measured in differentiated WT and gp91^{phox}-deficient PLB-985 cells. We hypothesize that the association of LBs with phagosomes is mediated by cytosolic phospholipase A2 (cPLA^2) and that release of AA by cPLA^2 near the phagocytic vacuole may be used to activate NADPH oxidase locally and/or to facilitate phagosome maturation. Work by Anes et al. (5), showing that selected lipids (including AA) activate actin assembly and phagosome maturation in macrophages infected with Mycobacterium tuberculosis and M. avium, lends some support for this hypothesis. Further studies, including experiments on cPLA^2-deficient PLB-985 cells, will be necessary to decipher the role of LBs in the innate immune response of phagocytes.

LIVE-CELL FLUORESCENCE MICROSCOPY ON PHAGOCYTES

The advent of genetically encoded protein-labeling procedures using autofluorescent proteins ("GFP technology") in the last decade has revolutionized cell biology by enabling dynamic optical microscopy on selectively labeled proteins in living cells (57). Techniques such as FRAP, fluorescence pho-

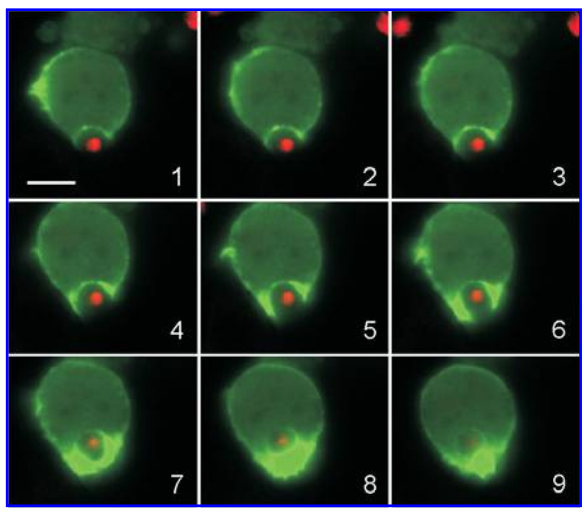

FIG. 6. Time-lapse fluorescence microscopy shows the translocation of p67^{phox}-EGFP to the nascent phagosome in PLB-985 cells stimulated with serum-opsonized zymosan particles. A series of fluorescence images (spanning 30 sec in total) is shown with the p67^{phox}-EGFP signal displayed in green and the weak autofluorescence of zymosan cores in red. The scale bar in image 1 represents 5 μm. (For interpretation of the references to color in this figure legend, the reader is referred to the web version of this article at www.liebertonline.com/ars.)

toactivation, and FCS reveal the intracellular location and movement of proteins, whereas close-range protein–protein interactions in living cells can be monitored with FRET microscopy and fluorescence lifetime imaging microscopy (FLIM) (99). However, the field of the phagocyte NADPH oxidase has been lagging behind in the application of GFP technology and advanced microscopy. This is because neutrophils are terminally differentiated cells and refractory to genetic manipulation. Therefore, nonphagocyte cell lines such as monkey kidney COS-7 and Chinese hamster ovary (CHO) cells have been used to express WT and mutant components of the phagocyte NADPH oxidase system and study their behavior using nonmicroscopic techniques (67) and, with GFP-technology, fluorescence microscopy (61). GFP labeling of subunits of other Nox family members in cell lines is also finding increased application. Finally, localized Rac activation dynamics can be visualized in living cells using FRET biosensors based on the binding of activated, GFP-labeled Rac to a p21-binding domain labeled with a suitable FRET acceptor. This elegant system, which has been applied to migrating neutrophils (34) and phagocytosing macrophages (45), might be used to study the relation between Rac activation and NADPH oxidase assembly and activation in living neutrophils.

A few cell types (available as cell lines) such as HL-60 and PLB-985 cells can be differentiated into neutrophil-like cells by induction with appropriate agents. Recently, we succeeded in stably expressing p67^{phox}-GFP and GFP-Rac2 in PLB-985 cells (91). Dynamic fluorescence microscopy on these cells allows us to study NADPH oxidase assembly in *bona fide* neutrophilic phagocytes, as discussed in the next section.

Fluorescence recovery after photobleaching on fluorescent cytosolic NADPH oxidase components: novel insights in translocation dynamics

To gain more insight into the process of translocation of the cytosolic NADPH oxidase components, EGFP-labeled versions of p67^{phox} and Rac2 were generated. These proteins were first tested for their capacity to support NADPH oxidase activity by transient expression in erythroleukemic K562 cells that contained all NADPH oxidase components (except p67^{phox} when p67^{phox}-EGFP was tested). Thereafter, these EGFP-labeled proteins were expressed in the myeloid cell line PLB-985. Time-lapse fluorescence microscopy revealed the translocation of p67^{phox}-EGFP and EGFP-Rac2 to the nascent phagosome in differentiated PLB-985 cells undergoing phagocytosis of zymosan particles, as reported here for p67^{phox}-EGFP in Fig. 6. Furthermore, expression of these constructs in gp91^{phox}-deficient PLB-985 cells and subsequent analysis of the translocation behavior of the fluorescent fusion proteins revealed that cyt b_{558} is essential for stable interaction of p67^{phox} and Rac2 with the phagosome, because these proteins were shed from the phagosome of gp91^{phox}-deficient PLB-985 cells after several minutes (91).

The retention time of these fusion proteins on zymosan-containing phagosomes was then studied by FRAP analysis, which is a well-established technique for studying diffusional processes of GFP fusion proteins inside living cells (58). The retention time of the p67^{phox}-EGFP as well as that of the EGFP-Rac2 fusion protein proved to be very short (~0.7 sec, ref. 91), which is firm proof for a high rate of exchange of these proteins at the phagosomal membrane. This was an unexpected result, because cyt b_{558} and the cytosolic components were believed to form a stable complex. However, our data indicate that the complex between cyt b_{558} and the cytosolic components associates and dissociates constantly, a cycle that might be driven by the switch of Rac2 between the GDP and the GTP-bound state. Future studies will reveal the molecular mechanisms that drive this cycle of association and dissociation. In addition, by combining Raman spectroscopy with fluorescence microscopy, it might be revealed whether the interaction between the cytosolic oxidase components is merely to activate cyt b_{558}, with activity being maintained when the complex dissociates, or, alternatively, that cyt b_{558} is active only when it physically interacts with the cytosolic components.

Fluorescence correlation spectroscopy: probing intracellular diffusion of cytosolic NADPH oxidase components

Fluorescence correlation spectroscopy (FCS) is a very sensitive technique to measure diffusion constants, binding interactions, and concentrations of fluorophores, including GFP fusion proteins, that are present at nanomolar to micromolar concentration inside living cells (42). It is based on the analysis of temporal fluctuations in fluorescence intensity as the fluorescent molecules of interest diffuse through a subfemtoliter confocal measurement volume. We have begun to characterize the diffusional behavior of GFP-labeled cytosolic NADPH oxidase subunits, expressed in PLB-985 cells (see previous section), using FCS on a home-built confocal fluorescence microscope with single-molecule sensitivity (79). Results from EGFP-Rac2 are presented here. As low fluorophore concentrations are required for FCS, unstimulated differentiated PLB-985 cells with low expression levels of EGFP-Rac2 were chosen for FCS measurements. Analysis of several 10-s fluorescence intensity time traces taken from the cytoplasm of PLB-985 cells revealed an average diffusion constant of 1.3×10^{-7} cm^2/sec for EGFP-Rac2 in resting cells, as calculated from the FCS autocorrelation plot displayed in Fig. 7. For comparison, plots for the fast-diffusing rhodamine 6G in water (2.8×10^{-6} cm^2/sec) and the slowly diffusing membrane dye DiO in the plasma membrane of neutrophils (0.7×10^{-8} cm$^{2/s}$) are also shown.

The diffusion constant for EGFP-Rac2 is slightly lower than previously reported values (ranging from 1.7×10^{-7} to 2.5×10^{-7} cm^2/sec) for free GFP diffusion in the cytoplasm of other cells (14, 18). This may be due to the coupling of GFP to Rac2, resulting in a bulkier fluorophore than GFP alone and consequently in a slower diffusion.

The initial results described here demonstrate the suitability of FCS for investigating NADPH oxidase in living cells. Current FCS experiments, directed toward the diffusion behavior of p67^{phox} and Rac2 in stimulated cells, will shed more light on the dynamics of NADPH oxidase assembly. Moreover, the use of fusion proteins of different color [*e.g.*, GFP and monomeric red fluorescent protein (mRFP)] in the same cell will enable dual-color fluorescence cross-correlation

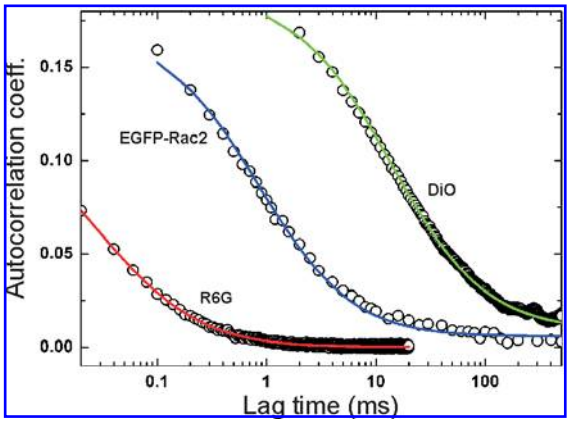

FIG. 7. Autocorrelation plots, calculated from FCS experiments, showing the diffusional behavior of rhodamine 6G in water (red), EGFP-Rac2 in the cytoplasm of unstimulated PLB-985 cells (blue), and DiO in the plasma membrane of neutrophils (green). It is clear that the diffusion time through the confocal measurement volume, determined as the lag time at which the autocorrelation coefficient has decreased to half its maximum value, is very different for these three cases. This is reflected by very different diffusion constants (see text). (For interpretation of the references to color in this figure legend, the reader is referred to the web version of this article at www.liebertonline.com/ars.)

spectroscopy (FCCS) on NADPH oxidase subunits. This technique complements FRET by measuring protein-protein interactions at very low concentrations inside cells.

OUTLOOK

Dynamic fluorescence microscopy and (resonant) Raman microscopy are powerful optical imaging tools to dissect molecular mechanisms of NADPH oxidase assembly and activation in phagocytes, as we have shown here. With the current technical status of live-cell fluorescence microscopy, several unresolved matters can be investigated. First, the dynamics of the interactions between $p67^{phox}$ and Rac2 in activated phagocytes can be monitored by the use of FRET or FCCS analysis, because both proteins can be labeled with different genetically encoded fluorescent tags without any deleterious effects on their function. The PLB-985 cell line offers an outstanding model system in which the interactions between these two molecules can be monitored, under conditions in which cyt b_{558} is present, as well as under conditions in which cyt b_{558} is absent (in cyt b_{558} knockout cells). Second, studies with this system will reveal the behavior of mutants of Rac2, $p67^{phox}$, and $gp91^{phox}$ in NADPH oxidase activation and will provide detailed information, relevant for CGD, on the molecular interactions that are affected by any of these mutations.

In addition to its ability to visualize the intracellular redox state of cyt b_{558} and the behavior of lipid bodies in phagocytes, Raman spectroscopy has the potential greatly to expand our knowledge of the widely expressed NADPH oxidases that are related to the phagocyte NADPH oxidase. Because specific antibodies against Noxes are not available, the label-free Raman technique can be instrumental to reveal the localization of a specific Nox in a particular cell type. Moreover, Raman imaging may allow the detection of the redox state of a given Nox, a feature that can be used to determine where and when the Nox of interest is active. These data can be used to address important questions about the function of the different Noxes, which, in some cases, is still obscure. In summary, single-cell optical-imaging techniques are becoming indispensable tools in increasing our understanding of the molecular mechanisms that take place in the phagocyte NADPH oxidase as well as in other Nox enzymes.

MATERIALS AND METHODS

Neutrophil isolation, cell culture, and opsonization of latex beads and zymosan particles

Peripheral blood from healthy adults and from a $p67^{phox}$-deficient ($A67^0$) CGD patient (a 22-year-old man) was obtained by venipuncture. Neutrophils were purified according to published procedures (74) and suspended in PBS/0.5% (wt/vol) BSA/0.38% trisodium citrate at ~5×10^6 cells/ml.

PLB-985 cells stably expressing $p67^{phox}$-EGFP and EGFP-Rac2 (91) were cultured in RPMI-1640 medium supplemented with 10% (vol/vol) fetal calf serum, 2 m*M* glutamine, penicillin (200 μg/ml), and streptomycin (200 μg/ml) in a CO_2 incubator at 37°C and passaged twice a week. PLB-985 cells were induced to differentiate into neutrophilic granulocytes by the addition of 0.5% (vol/vol) *N*,*N*-dimethylformamide (DMF) to dilute cell suspensions (~2×10^5 cells/ml) in culture medium and incubation for 6 days.

Latex beads (diameter 1.0 μm; Polysciences, Warrington, PA) and zymosan particles (Sigma-Aldrich, Zwijndrecht, The Netherlands) were opsonized with fresh human serum for 1 h at 37°C, washed 2× with PBS, and resuspended in PBS.

Resonant Raman spectroscopy and microscopy on neutrophils

Resonant Raman experiments on neutrophils were performed on a home-built laser-scanning confocal Raman microspectrometer using 413.1-nm excitation provided by a Kr^+ laser (Innova 90-K; Coherent, Santa Clara, CA), as described elsewhere (94). For live-cell Raman spectroscopy on quiescent WT and $A67^0$ neutrophils, cells were adhered for 15 min to poly-L-lysine-coated CaF_2 disks, incubated in phagocytosis buffer [PBS/1 m*M* $CaCl_2$/0.5 m*M* $MgCl_2$/5 m*M* glucose/0.2% (wt/vol) BSA], and directly subjected to Raman spectroscopy. Live-cell Raman spectroscopy on phagocytosing WT and $A67^0$ neutrophils was performed by adhering cells to poly-L-lysine–coated CaF_2, incubating them with opsonized latex beads for 30 min at 37°C to allow phagocytosis, and subjecting them to Raman spectroscopy. Raman spectra from individual live cells were recorded by scanning the laser beam, focused to a diffraction-limited spot of 0.32 μm in diameter by a 63×/1.2 NA water-immersion objective (Plan Neofluar; Carl Zeiss, Jena, Germany), over a cellular area of 8×8 μm^2 and accumulating the Raman signal for 5 sec at 1-mW excitation power. Mean spectra from every type of neutrophil (WT

and A67^0 CGD cells, both quiescent and phagocytosing) were determined by averaging spectra from 25 different cells. To allow comparison between different cell types, the Raman spectra shown in Fig. 3 were subtracted and scaled on their 676 cm^{-1} band.

To visualize the cyt b_{558} distribution in phagocytosing A67^0 CGD neutrophils, we performed resonant Raman imaging experiments on cells that had adhered to poly-L-lysine–coated CaF_2 disks, incubated with opsonized latex beads for 30 min at 37°C, washed with PBS, and fixed for 1 h in 2% paraformaldehyde at room temperature. For imaging experiments on quiescent A67^0 CGD neutrophils, the phagocytosis step was omitted. Raman imaging experiments, data processing, and hierarchical cluster analysis of Raman data sets were performed as described (93–95).

Nonresonant Raman microscopy on phagocytosing neutrophils

Nonresonant Raman imaging experiments on neutrophils were performed on the same confocal Raman microspectrometer as described earlier using 647.1-nm excitation (provided by a Kr^+ laser; Innova 90-K, Coherent) instead of 413.1 nm. To investigate the association of intracellular AA-containing lipid bodies (LBs) with phagocytosed zymosan particles, a procedure similar to that previously reported for the study of LB association with phagocytosed latex beads (95) was followed. In brief, adhered neutrophils were incubated for 1 h with octadeuterated arachidonic acid (AA-d_8), washed with phagocytosis buffer, incubated for 30 min at 37°C with opsonized zymosan particles, and fixed with 2% paraformaldehyde for 30 min at room temperature. Nonresonant Raman imaging experiments on this sample (1-sec accumulation time per image pixel at 100-mW excitation power), data processing, and analysis were performed as described (95).

Fluorescence microscopy on EGFP-Rac2 PLB-985 cells

Differentiated PLB-985 cells expressing p67^{phox}-EGFP were allowed to adhere to glass coverslips in RPMI medium at 37°C in a heated stage on an LSM510 confocal laser scanning microscope (Carl Zeiss, Göttingen, Germany) for 5 min before serum-opsonized zymosan particles were added. Translocation of p67^{phox}-EGFP to nascent phagosomes was visualized by recording time-lapse confocal fluorescence images (see Fig. 6) with 488-nm excitation from an Ar^+ laser.

Fluorescence correlation spectroscopy experiments on PLB-985 cells expressing EGFP-Rac2 were performed on a home-built confocal fluorescence microscope with single-molecule sensitivity, which was described in detail (79). Fluorescence-intensity time traces were obtained from unstimulated PLB-985 cells with a low expression level of EGFP-Rac2 by positioning the 488-nm laser beam in various cytoplasmic locations and recording 10-sec streams of emitted photons. Time traces with a 100-μsec time resolution were processed offline by autocorrelation analysis, and the resulting autocorrelation plots were fitted with a model for 3D translational diffusion to derive EGFP-Rac2 diffusion constants (for a general introduction to FCS procedures; see ref. 100).

ACKNOWLEDGMENTS

Financial support from the Chronic Granulomatous Disorder Research Trust (U.K.) and the Landsteiner Foundation for Blood Transfusion Research (The Netherlands) is gratefully acknowledged.

ABBREVIATIONS

AA, arachidonic acid; CGD, chronic granulomatous disease; cyt b_{558}, flavocytochrome b_{558}; FCS, fluorescence correlation spectroscopy; FRAP, fluorescence recovery after photobleaching; FRET, Förster resonance energy transfer; (E)GFP, (enhanced) green fluorescent protein; MPO, myeloperoxidase; ROS, reactive oxygen species; RR, resonant Raman.

REFERENCES

1. Ahluwalia J, Tinker A, Clapp LH, Duchen MR, Abramov AY, Pope S, Nobles M, and Segal AW. The large-conductance Ca^{2+}-activated K^+ channel is essential for innate immunity. *Nature* 427: 853–858, 2004.
2. Allen L-AH, DeLeo FR, Gallois A, Toyoshima S, Suzuki K, and Nauseef WM. Transient association of the nicotinamide dinucleotide phosphate oxidase subunits p47*phox* and p67*phox* with phagosomes in neutrophils from patients with X-linked chronic granulomatous disease. *Blood* 93: 3521–3530, 1999.
3. Ambruso DR, Cusack N, and Thurman G. NADPH oxidase activity of neutrophil specific granules: requirement for cytosolic components and evidence of assembly during cell activation. *Mol Genet Metab* 81: 313–321, 2004.
4. Andersen JK. Oxidative stress in neurodegeneration: cause or consequence? *Nat Rev Neurosci* 5: S18–S25, 2004.
5. Anes E, Kühnel MP, Bos E, Moniz-Pereira J, Habermann A, and Griffiths G. Selected lipids activate phagosome actin assembly and maturation resulting in killing of pathogenic mycobacteria. *Nat Cell Biol* 5: 793–802, 2003.
6. Babior BM. NADPH oxidase: an update. *Blood* 93: 1464–1476, 1999.
7. Babior BM. Phagocytes and oxidative stress. *Am J Med* 109: 33–44, 2000.
8. Bainton DF and Farquhar MG. Origin of granules in polymorphonuclear granulocytes: two types derived from opposite faces of the Golgi complex in developing granulocytes. *J Cell Biol* 28: 277–301, 1966.
9. Biberstine-Kinkade KJ, DeLeo FR, Epstein RI, LeRoy BA, Nauseef WM, and Dinauer MC. Heme-ligating histidines in flavocytochrome b_{558}: identification of specific histidines in gp91^{phox}. *J Biol Chem* 276: 31105–31112, 2001.
10. Bokoch GM and Diebold BA. Current molecular models for NADPH oxidase regulation by Rac GTPase. *Blood* 100: 2692–2696, 2002.
11. Borregaard N, Heiple JM, Simons ER, and Clark RA. Subcellular localization of the b-cytochrome component of the human neutrophil microbicidal oxidase: translocation during activation. *J Cell Biol* 97: 52–61, 1983.

12. Bozza PT and Bandeira-Melo C. Mechanisms of leukocyte lipid body formation and function in inflammation. *Mem Inst Oswaldo Cruz* 100(suppl I): 113–120, 2005.
13. Brederoo P, van der Meulen J, and Mommaas-Kienhuis AM. Development of the granule population in neutrophil granulocytes from human bone marrow. *Cell Tissue Res* 234: 469–496, 1983.
14. Brock R, Vàmosi G, Vereb G, and Jovin TM. Rapid characterization of green fluorescent protein fusion proteins on the molecular and cellular level by fluorescence correlation microscopy. *Proc Natl Acad Sci U S A* 96: 10123–10128, 1999.
15. Brown GE, Stewart MQ, Liu H, Ha V-L, and Yaffe MB. A novel assay system implicates PtdIns(3,4)P_2, PtdIns(3)P, and PKCδ in intracellular production of reactive oxygen species by the NADPH oxidase. *Mol Cell* 11: 35–47, 2003.
16. Carey PR. Raman spectroscopy, the sleeping giant in structural biology, awakes. *J Biol Chem* 274: 26625–26628, 1999.
17. Carlyon JA, Abdel Latif D, Pypaert M, Lacy P, and Fikrig E. *Anaplasma phagocytophilum* utilizes multiple host evasion mechanisms to thwart NADPH oxidase-mediated killing during neutrophil infection. *Infect Immun* 72: 4772–4783, 2004.
18. Chen Y, Müller JD, Ruan Q, and Gratton E. Molecular brightness characterization of EGFP in vivo by fluorescence fluctuation spectroscopy. *Biophys J* 82: 133–144, 2002.
19. Choo-Smith L-P, Edwards HGM, Endtz HP, Kros JM, Heule F, Barr H, Robinson Jr. JS, Bruining HA, and Puppels GJ. Medical applications of Raman spectroscopy: from proof of principle to clinical implementation. *Biopolymers (Biospectroscopy)* 67: 1–9, 2002.
20. Clark RA, Leidal KG, Pearson DW, and Nauseef WM. NADPH oxidase of human neutrophils: subcellular localization and characterization of an arachidonate-activatable superoxide-generating system. *J Biol Chem* 262: 4065–4074, 1987.
21. Cross AR and Segal AW. The NADPH oxidase of professional phagocytes: prototype of the NOX electron transport chain systems. *Biochim Biophys Acta* 1657: 1–22, 2004.
22. Dana R, Leto TL, Malech HL, and Levy R. Essential requirement of cytosolic phospholipase A_2 for activation of the phagocyte NADPH oxidase. *J Biol Chem* 273: 441–445, 1998.
23. Deane JA and Fruman DA. Phosphoinositide 3-kinase: diverse roles in immune cell activation. *Annu Rev Immunol* 22: 563–598, 2004.
24. DeCoursey TE, Morgan D, and Cherny VV. The gp91^{phox} component of NADPH oxidase is not a voltage-gated proton channel. *J Gen Physiol* 120: 773–779, 2002.
25. DeCoursey TE. Voltage-gated proton channels and other proton transfer pathways. *Physiol Rev* 83: 475–579, 2003.
26. DeCoursey TE and Ligeti E. Regulation and termination of NADPH oxidase activity. *Cell Mol Life Sci* 62: 2173–2193, 2005.
27. DeLeo FR, Allen L-AH, Apicella MA, and Nauseef WM. NADPH oxidase activation and assembly during phagocytosis. *J Immunol* 163: 6732–6740, 1999.
28. Diem M, Romeo M, Boydston-White S, Miljkovi[cacute] M, and Matthäus C. A decade of vibrational microspectroscopy of human cells and tissue (1994-2004). *Analyst* 129: 880–885, 2004.
29. Dvorak AM, Dvorak HF, Peters SP, Shulman ES, MacGlashan DW Jr, Pyne K, Harvey VS, Galli SJ, and Lichtenstein LM. Lipid bodies: cytoplasmic organelles important to arachidonate metabolism in macrophages and mast cells. *J Immunol* 131: 2965–2976, 1983.
30. Faurschou M and Borregaard N. Neutrophil granules and secretory vesicles in inflammation. *Microbes Infect* 5: 1317–1327, 2003.
31. Fernandez DC, Bhargava R, Hewitt SM, and Levin IW. Infrared spectroscopic imaging for histopathologic recognition. *Nat Biotechnol* 23: 469–474, 2005.
32. Fujii H, Finnegan MG, Miki T, Crouse BR, Kakinuma K, and Johnson MK. Spectroscopic identification of the heme axial ligation of cytochrome b_{558} in the NADPH oxidase of porcine neutrophils. *FEBS Lett* 377: 345–348, 1995.
33. Gallois A, Klein JR, Allen L-A H, Jones BD, and Nauseef WM. *Salmonella* pathogenicity island 2-encoded type III secretion system mediates exclusion of NADPH oxidase assembly from the phagosomal membrane. *J Immunol* 166: 5741–5748, 2001.
34. Gardiner EM, Pestonjamasp KN, Bohl BP, Chamberlain C, Hahn KM, and Bokoch GM. Spatial and temporal analysis of Rac activation during live neutrophil chemotaxis. *Curr Biol* 12: 2029–2034, 2002.
35. Ginsel LA, Onderwater JJM, Fransen JAM, Verhoeven AJ, and Roos D. Localization of the low-M_r subunit of cytochrome b_{558} in human blood phagocytes by immunoelectron microscopy. *Blood* 76: 2105–2116, 1990.
36. Groemping Y and Rittinger K. Activation and assembly of the NADPH oxidase: a structural perspective. *Biochem J* 386: 401–416, 2005.
37. Grogan A, Reeves E, Keep N, Wientjes F, Totty NF, Burlingame AL, Hsuan JJ, and Segal AW. Cytosolic *phox* proteins interact with and regulate the assembly of coronin in neutrophils. *J Cell Sci* 110: 3071–3081, 1997.
38. Guichard C, Pedruzzi E, Dewas C, Fay M, Pouzet C, Bens M, Vandewalle A, Ogier-Denis E, Gougerot-Pocidalo M-A, and Elbim C. Interleukin-8-induced priming of neutrophil oxidative burst requires sequential recruitment of NADPH oxidase components into lipid rafts. *J Biol Chem* 280: 37021–37032, 2005.
39. Haka AS, Shafer-Peltier KE, Fitzmaurice M, Crowe J, Dasari RR, and Feld MS. Diagnosing breast cancer using Raman spectroscopy. *Proc Natl Acad Sci U S A* 102: 12371–12376, 2005.
40. Hanlon EB, Manoharan R, Koo T-W, Shafer KE, Motz JT, Fitzmaurice M, Kramer JR, Itzkan I, Dasari RR, and Feld MS. Prospects for *in vivo* Raman spectroscopy. *Phys Med Biol* 45: R1–R59, 2000.
41. Henderson LM and Meech RW. Proton conduction through gp91^{phox}. *J Gen Physiol* 120: 759–765, 2002.
42. Hess ST, Huang S, Heikal AA, and Webb WW. Biological and chemical applications of fluorescence correlation spectroscopy: a review. *Biochemistry* 41: 697–705, 2002.
43. Heyworth PG, Curnutte JT, Nauseef WM, Volpp BD, Pearson DW, Rosen H, and Clark RA. Neutrophil nicotinamide adenine dinucleotide phosphate oxidase assembly: translocation of p47-*phox* and p67-*phox* requires interaction be-

tween p47-*phox* and cytochrome b_{558}. *J Clin Invest* 87: 352–356, 1991.
44. Heyworth PG, Cross AR, and Curnutte JT. Chronic granulomatous disease. *Curr Opin Immunol* 15: 578–584, 2003.
45. Hoppe AD and Swanson JA. Cdc42, Rac1, and Rac2 display distinct patterns of activation during phagocytosis. *Mol Biol Cell* 15: 3509–3519, 2004.
46. Hurst JK, Loehr TM, Curnutte JT, and Rosen H. Resonance Raman and electron paramagnetic resonance structural investigations of neutrophil cytochrome b_{558}. *J Biol Chem* 266: 1627–1634, 1991.
47. Ido JW and Mueller AC. Neutrophil NADPH oxidase is reduced at the *Anaplasma phagocytophilum* phagosome. *Infect Immun* 72: 5392–5401, 2004.
48. Ischiropoulos H and Beckman JS. Oxidative stress and nitration in neurodegeneration: cause, effect, or association? *J Clin Invest* 111: 163–169, 2003.
49. Jesaitis AJ, Buescher ES, Harrison D, Quinn MT, Parkos CA, Livesey S, and Linner J. Ultrastructural localization of cytochrome *b* in the membranes of resting and phagocytosing human granulocytes. *J Clin Invest* 85: 821–835, 1990.
50. Karlsson A and Dahlgren C. Assembly and activation of the neutrophil NADPH oxidase in granule membranes. *Antiox Redox Signal* 4: 49–60, 2002.
51. Kindzelskii AL and Petty HR. Apparent role of traveling metabolic waves in oxidant release by living neutrophils. *Proc Natl Acad Sci U S A* 99: 9207–9212, 2002.
52. Kindzelskii AL and Petty HR. Fluorescence spectroscopic detection of mitochondrial flavoprotein redox oscillations and transient reduction of the NADPH oxidase-associated flavoprotein in leukocytes. *Eur Biophys J* 33: 291–299, 2004.
53. Kobayashi T, Robinson JM, and Seguchi H. Identification of intracellular sites of superoxide production in stimulated neutrophils. *J Cell Sci* 111: 81–91, 1998.
54. Lambeth JD. Nox enzymes and the biology of reactive oxygen. *Nat Rev Immunol* 4: 181–189, 2004.
55. Lee WL, Harrison RE, and Grinstein S. Phagocytosis by neutrophils. *Microbes Infect* 5: 1299–1306, 2003.
56. Levin IW and Bhargava R. Fourier transform infrared vibrational spectroscopic imaging: integrating microscopy and molecular recognition. *Annu Rev Phys Chem* 56: 429–474, 2005.
57. Lippincott-Schwartz J and Patterson GH. Development and use of fluorescent protein markers in living cells. *Science* 300: 87–91, 2003.
58. Lippincott-Schwartz J, Snapp E, and Kenworthy A. Studying protein dynamics in living cells. *Nat Rev Mol Cell Biol* 2: 444–456, 2001.
59. Lundqvist H, Follin P, Khalfan L, and Dahlgren C. Phorbol myristate acetate-induced NADPH oxidase activity in human neutrophils: only half the story has been told. *J Leukoc Biol* 59: 270–279, 1996.
60. Melo RCN, D'Ávila H, Fabrino DL, Almeida PE, and Bozza PT. Macrophage lipid body induction by Chagas disease in vivo: putative intracellular domains for eicosanoid formation during infection. *Tissue Cell* 35: 59–67, 2003.
61. Murillo I and Henderson LM. Expression of gp91^{phox}/Nox2 in COS-7 cells: cellular localization of the protein and the detection of outward proton currents. *Biochem J* 385: 649–657, 2005.
62. Nisimoto Y, Motalebi S, Han C-H, and Lambeth JD. The p67^{phox} activation domain regulates electron flow from NADPH to flavin in flavocytochrome b_{558}. *J Biol Chem* 274: 22999–23005, 1999.
63. Notingher I, Bisson I, Bishop AE, Randle WL, Polak JMP, and Hench LL. In situ spectral monitoring of mRNA translation in embryonic stem cells during differentiation in vitro. *Anal Chem* 76: 3185–3193, 2004.
64. Otto C, Sijtsema NM, and Greve J. Confocal Raman microspectroscopy of the activation of single neutrophilic granulocytes. *Eur Biophys J* 27: 582–589, 1998.
65. Perisic O, Wilson MI, Karathanassis D, Bravo J, Pacold ME, Ellson CD, Hawkins PT, Stephens L, and Williams RL. The role of phosphoinositides and phosphorylation in regulation of NADPH oxidase. *Adv Enzyme Regul* 44: 279–298, 2004.
66. Petry R, Schmitt M, and Popp J. Raman spectroscopy: a prospective tool in the life sciences. *Chem Phys Chem* 4: 14–30, 2003.
67. Price MO, McPhail LC, Lambeth JD, Han C-H, Knaus UG, and Dinauer MC. Creation of a genetic system for analysis of the phagocyte respiratory burst: high-level reconstitution of the NADPH oxidase in a nonhematopoietic system. *Blood* 99: 2653–2661, 2002.
68. Puppels GJ, de Mul FFM, Otto C, Greve J, Robert-Nicoud M, Arndt-Jovin DJ, and Jovin TM. Studying single living cells and chromosomes by confocal Raman microspectroscopy. *Nature* 347: 301–303, 1990.
69. Puppels GJ, Garritsen HSP, Segers-Nolten GMJ, De Mul FFM, and Greve J. Raman microspectroscopic approach to the study of human granulocytes. *Biophys J* 60: 1046–1056, 1991.
70. Quinn MT and Gauss KA. Structure and regulation of the neutrophil respiratory burst oxidase: comparisons with nonphagocyte oxidases. *J Leukoc Biol* 76: 760–781, 2004.
71. Rada BK, Geiszt M, Káldi K, Timár C, and Ligeti E. Dual role of phagocytic NADPH oxidase in bacterial killing. *Blood* 104: 2947–2953, 2004.
72. Reeves EP, Lu H, Lortat Jacobs H, Messina CGM, Bolsover S, Gabella G, Potma EO, Warley A, Roes J, and Segal AW. Killing activity of neutrophils is mediated through activation of proteases by K^+ flux. *Nature* 416: 291–297, 2002.
73. Robinson JM, Ohira T, and Badwey JA. Regulation of the NADPH-oxidase complex of phagocytic leukocytes: recent insights from structural biology, molecular genetics, and microscopy. *Histochem Cell Biol* 122: 293–304, 2004.
74. Roos D and de Boer M. Purification and cryopreservation of phagocytes from human blood. *Methods Enzymol* 132: 225–243, 1986.
75. Roos D, de Boer M, Kuribayashi F, Meischl C, Weening RS, Segal AW, Åhlin A, Nemet K, Hossle JP, Bernatowska-Matuszkiewics E, and Middleton-Price H. Mutations in the X-linked and autosomal recessive forms of chronic granulomatous disease. *Blood* 87: 1663–1681, 1996.
76. Roos D, van Bruggen R, and Meischl C. Oxidative killing of microbes by neutrophils. *Microbes Infect* 5: 1307–1315, 2003.

77. Segal AW, Dorling J, and Coade S. Kinetics of fusion of the cytoplasmic granules with phagocytic vacuoles in human polymorphonuclear leukocytes. *J Cell Biol* 85: 42–59, 1980.
78. Segal AW. How neutrophils kill microbes. *Annu Rev Immunol* 23: 197–223, 2005.
79. Segers-Nolten GMJ, Wyman C, Wijgers N, Vermeulen W, Lenferink ATM, Hoeijmakers JHJ, Greve J, and Otto C. Scanning confocal fluorescence microscopy for single molecule analysis of nucleotide excision repair complexes *Nucleic Acids Res* 30: 4720–4727, 2002.
80. Shmelzer Z, Haddad N, Admon E, Pessach I, Leto TL, Eitan-Hazan Z, Hershfinkel M, and Levy R. Unique targeting of cytosolic phospholipase A_2 to plasma membranes mediated by the NADPH oxidase in phagocytes. *J Cell Biol* 162: 683–692, 2003.
81. Sijtsema NM, Otto C, Segers-Nolten GMJ, Verhoeven AJ, and Greve J. Resonance Raman microspectroscopy of myeloperoxidase and cytochrome b_{558} in human neutrophilic granulocytes. *Biophys J* 74: 3250–3255, 1998.
82. Sijtsema NM, Tibbe AGJ, Segers-Nolten IGMJ, Verhoeven AJ, Weening RS, Greve J, and Otto C. Intracellular reactions in single human granulocytes upon phorbol myristate acetate activation using confocal Raman microspectroscopy. *Biophys J* 78: 2606–2613, 2000.
83. Simons K and Toomre D. Lipid rafts and signal transduction. *Nat Rev Mol Cell Biol* 1: 31–41, 2000.
84. Spiro TG and Czernuszewicz RS. Resonance Raman spectroscopy of metalloproteins. *Methods Enzymol* 246: 416–460, 1995.
85. Stephens L, Ellson C, and Hawkins P. Roles of PI3Ks in leukocyte chemotaxis and phagocytosis. *Curr Opin Cell Biol* 14: 203–213, 2002.
86. Stuart LM and Ezekowitz RAB. Phagocytosis: elegant complexity. *Immunity* 22: 539–550, 2005.
87. Tarpey MM, Wink DA, and Grisham MB. Methods for detection of reactive metabolites of oxygen and nitrogen: *in vitro* and *in vivo* considerations. *Am J Physiol Regul Integr Comp Physiol* 286: R431–R444, 2004.
88. Underhill DM and Ozinsky A. Phagocytosis of microbes: complexity in action. *Annu Rev Immunol* 20: 825–852, 2002.
89. Uzunbajakava N, Lenferink A, Kraan Y, Volokhina E, Vrensen G, Greve J, and Otto C. Nonresonant confocal Raman imaging of DNA and protein distribution in apoptotic cells. *Biophys J* 84: 3968–3981, 2003.
90. Vaissiere C, Le Cabec V, and Maridonneau-Parini I. NADPH oxidase is functionally assembled in specific granules during activation of human neutrophils. *J Leukoc Biol* 65: 629–634, 1999.
91. Van Bruggen R, Anthony E, Fernandez-Borja M, and Roos D. Continuous translocation of Rac2 and the NADPH oxidase component $p67^{phox}$ during phagocytosis. *J Biol Chem* 279: 9097–9102, 2004.
92. Van de Poll SW, Römer TJ, Puppels GJ, and van der Laarse A. Raman spectroscopy of atherosclerosis. *J Cardiovasc Risk* 9: 255–261, 2002.
93. Van Manen H-J, Uzunbajakava N, Van Bruggen R, Roos D, and Otto C. Resonance Raman imaging of the NADPH oxidase subunit cytochrome b_{558} in single neutrophilic granulocytes. *J Am Chem Soc* 125: 12112– 12113, 2003.
94. Van Manen H-J, Kraan YM, Roos D, and Otto C. Intracellular chemical imaging of heme-containing enzymes involved in innate immunity using resonance Raman microscopy. *J Phys Chem B* 108: 18762–18771, 2004.
95. Van Manen H-J, Kraan YM, Roos D, and Otto C. Single-cell Raman and fluorescence microscopy reveal the association of lipid bodies with phagosomes in leukocytes. *Proc Natl Acad Sci U S A* 102: 10159–10164, 2005.
96. Vazquez-Torres A, Xu Y, Jones-Carson J, Holden DW, Lucia SM, Dinauer MC, Mastroeni P, and Fang FC. *Salmonella* pathogenicity island 2-dependent evasion of the phagocyte NADPH oxidase. *Science* 287: 1655–1658, 2000.
97. Vieira OV, Botelho RJ, and Grinstein S. Phagosome maturation: aging gracefully. *Biochem J* 366: 689–704, 2002.
98. Vignais PV. The superoxide-generating NADPH oxidase: structural aspects and activation mechanism. *Cell Mol Life Sci* 59: 1428–1459, 2002.
99. Wallrabe H and Periasamy A. Imaging protein molecules using FRET and FLIM microscopy. *Curr Opin Biotechnol* 16: 19–27, 2005.
100. Widengren J and Mets Ü. Conceptual basis of fluorescence correlation spectroscopy and related techniques as tools in bioscience. In: Zander C, Enderstein J, Keller RA (Eds). *Single molecule detection in solution*: *methods and applications.* Wiley-VCH, Berlin, 2002, pp. 69–120.
101. Yeung T, Touret N, and Grinstein S. Quantitative fluorescence microscopy to probe intracellular microenvironments. *Curr Opin Microbiol* 8: 350–358, 2005.

Address reprint requests to:
Henk-Jan van Manen
Biophysical Engineering Group
Faculty of Science & Technology
Institute for Biomedical Technology (BMTI)
MESA+ Institute for Nanotechnology, University of Twente
P.O. Box 217
7500 AE Enschede, The Netherlands

E-mail: h.w.j.vanmanen@tnw.utwente.nl

First submission to ARS Central, April 27, 2006; date of acceptance, April 29, 2006.

This article has been cited by:

1. Toru Sasaki, Takahiko Shimizu, Tomoko Koyama, Masanobu Sakai, Satoshi Uchiyama, Satoru Kawakami, Yoshihiro Noda, Takuji Shirasawa, Shuji Kojima. 2011. Superoxide dismutase deficiency enhances superoxide levels in brain tissues during oxygenation and hypoxia-reoxygenation. *Journal of Neuroscience Research* **89**:4, 601-610. [CrossRef]
2. Asma Tlili, Sophie Dupré-Crochet, Marie Erard, Oliver Nüße. 2011. Kinetic analysis of phagosomal production of reactive oxygen species. *Free Radical Biology and Medicine* **50**:3, 438-447. [CrossRef]
3. John M. Robinson. 2008. Reactive oxygen species in phagocytic leukocytes. *Histochemistry and Cell Biology* **130**:2, 281-297. [CrossRef]
4. F.L. Crane, H. Low. 2008. Reactive oxygen species generation at the plasma membrane for antibody control. *Autoimmunity Reviews* **7**:7, 518-522. [CrossRef]
5. Henk-Jan van Manen, Paul Verkuijlen, Paul Wittendorp, Vinod Subramaniam, Timo K. van den Berg, Dirk Roos, Cees Otto. 2008. Refractive Index Sensing of Green Fluorescent Proteins in Living Cells Using Fluorescence Lifetime Imaging Microscopy. *Biophysical Journal* **94**:8, L67-L69. [CrossRef]
6. Jie Wang, Lingna Li, Hui Cang, Guiying Shi, Jing Yi. 2008. NADPH oxidase-derived reactive oxygen species are responsible for the high susceptibility to arsenic cytotoxicity in acute promyelocytic leukemia cells. *Leukemia Research* **32**:3, 429-436. [CrossRef]
7. E Eriksson, J Scrimgeour, A Granéli, K Ramser, R Wellander, J Enger, D Hanstorp, M Goksör. 2007. Optical manipulation and microfluidics for studies of single cell dynamics. *Journal of Optics A: Pure and Applied Optics* **9**:8, S113-S121. [CrossRef]
8. Kathy K. Griendling . 2006. NADPH Oxidases: New Regulators of Old Functions. *Antioxidants & Redox Signaling* **8**:9-10, 1443-1445. [Citation] [Full Text PDF] [Full Text PDF with Links]